A Simple Way of Synthesizing Single-Crystalline Semiconducting Copper Sulfide Nanorods by Using Ultrasonication during Template-Assisted Electrodeposition

Krishna V. Singh,[†,#] Alfredo A. Martinez-Morales,[‡,#] G. T. Senthil Andavan,[‡,§] Krassimir N. Bozhilov,[||] and Mihrimah Ozkan*[,‡]

Department of Chemical & Environmental Engineering, Department of Electrical Engineering, Center for Nanoscale Science and Engineering, and Department of Earth Sciences, University of California, Riverside, California 92521

Received December 11, 2006. Revised Manuscript Received March 14, 2007

We demonstrate here the utilization of ultrasonication during template-assisted electrodeposition to synthesize high quality one-dimensional nanostructures. Copper sulfide nanorods were synthesized "sonoelectrochemically" to achieve single-crystal nanorods with predominantly single stoichiometric composition (1.0:1.0 Cu:S). Structural characterization by HRTEM, SAD, EDS reveals that nanorods have fully crystalline hexagonal covellite (CuS) structure, which is topotactically intergrown with minor amounts of nanometer size domains of cubic $Cu_{1.8}S$. Nanorods in the range of 50−200 nm in diameter were produced and electrically characterized as p-type semiconductors.

Introduction

Template-assisted electrochemical deposition has been one of the widely investigated and exploited synthesis processes for one-dimensional nanostructures.[1,2] However, reports on analyzing the potential benefits of combining ultrasonication with electrochemistry, sonoelectrochemistry, are very few.[3−5] The underlying process in ultrasonication is acoustic cavitation: the formation, growth, and implosive collapse of bubbles inside the liquid.[6] Cavitation serves as the means of concentrating diffuse energy of sound in a small bubble. The release of this energy results in the formation of localized spots of high-temperature ($T \approx 5000$ °C) and pressure.[6] This unique interaction of energy and matter during ultrasonication process results in several benefits for the electrochemical deposition process. Primarily, these benefits fall into three categories: (1) reduction in mass-transfer resistance by decreasing the Nernst diffusion layer from 200 μm down to 3.5−20 μm;[7] (2) cleaning of the electrode surface by removal of contaminants and gases;[5] and (3) increase in reaction rate by localized heating and high-pressure fields.[6]

Here, we demonstrate the synthesis of copper sulfide nanorods by sonoelectrochemistry due to its utility in semiconducting, chemical, and photovoltaic applications.[8−10] Various forms of copper sulfide have been reported in the literature,[11−14] but one-dimensional (1D) nanostructures have invoked a keen interest recently. Different synthesis routes were developed for the synthesis of copper sulfide nanorods/wires/tubes, including the organic-amine-assisted hydrothermal method,[15] starting from single-source precursor Cu-dithiooxamide,[16] surfactant- or oxide-assisted growth from the copper surface under a hydrogen sulfide atmosphere[17,18] and sulfur source,[19] and from thermal decomposition of CuS_2CNEt_2 in a binary surfactant solvent.[20] Fabrication of copper sulfide nanowires in Na-4 mica by an ion-exchange reaction and growth of microtubes is also reported.[21,22] The number of undesired limitations with these approaches, such as the

* Corresponding author. E-mail: mihri@ee.ucr.edu. Phone: (951) 827-2900.
† Department of Chemical & Environmental Engineering, University of California, Riverside.
# These authors contributed equally to this work.
‡ Department of Electrical Engineering, University of California, Riverside.
§ Center for Nanoscale Science and Engineering, University of California, Riverside.
|| Department of Earth Sciences, University of California, Riverside.

(1) Martin, C. R. *Science* **1994**, *266* (5193), 1961−1966.
(2) Schonenberger, C.; van der Zande, B. M. I.; Fokkink, L. G. J.; Henny, M.; Schmid, C.; Kruger, M.; Bachtold, A.; Huber, R.; Birk, H.; Staufer, U. *J. Phys. Chem. B* **1997**, *101* (28), 5497−5505.
(3) Dobrev, D.; Vetter, J.; Angert, N.; Neumann, R. *Appl. Phys. A: Mater. Sci. Process.* **1999**, *69* (2), 233−237.
(4) Atobe, M.; Tsuji, H.; Asami, R.; Fuchigami, T. *J. Electrochem. Soc.* **2006**, *153* (1), D10−D13.
(5) Haas, I.; Gedanken, A. *Chem. Mater.* **2006**, *18* (5), 1184−1189.
(6) Suslick, K. S. *Science* **1990**, *247* (4949), 1439−1445.
(7) Compton, R. G.; Eklund, J. C.; Marken, F. *Electroanalysis* **1997**, *9* (7), 509−522.
(8) Bragagnolo, J. A.; Barnett, A. M.; Phillips, J. E.; Hall, R. B.; Rothwarf, A.; Meakin, J. D. *IEEE Trans. Electron Devices* **1980**, *27*, 645−651.
(9) Piao, Y.; Lim, H.; Chang, J. Y.; Lee, W.; Kim, H. *Electrochim. Acta* **2005**, *50*, 2997−3013.
(10) Chen, J.; Deng, S. Z.; Xu, N. S.; Wang, S.; Wen, X.; Yang, S.; Yang, C.; Wang, J.; Weikun, G. *Appl. Phys. Lett.* **2002**, *80*, 3620−3622.
(11) (a) Dhar, S.; Chakrabarti, S. *J. Appl. Phys.* **1997**, *82*, 655−657. (b) Wu, C.; Yu, S.; Antonietti, M. *Chem. Mater.* **2006**, *18*, 3599−3601
(12) Gao, L.; Wang, E. B.; Lian, S. Y.; Kang, Z. H.; Lan, Y.; Wu, D. *Solid State Commun.* **2004**, *130* (5), 309−312.
(13) Grijalva, H.; Inoue, M.; Boggavarapu, S.; Calvert, P. *J. Mater. Chem.* **1996**, *6* (7), 1157−1160.
(14) Gautam, U. K.; Mukherjee, B. *Bull. Mater. Sci.* **2006**, *29* (1), 1−5.
(15) Lu, Q. Y.; Gao, F.; Zhao, D. Y. *Nano Lett.* **2002**, *2* (7), 725−728.
(16) Roy, P.; Srivastava, S. K. *Cryst. Growth Des.* **2006**, *6* (8), 1921−1926.
(17) Wang, S. H.; Yang, S. H. *Chem. Phys. Lett.* **2000**, *322*, 567−571.
(18) Wang, N.; Fung, K. K.; Wang, S.;Yang, S. *J. Cryst. Growth* **2001**, *233*, 226−232.
(19) Wu, C. Y.; Yu, S. H.; Chen, S. F.; Liu, G. N.; Liu, B. H. *J. Mater. Chem.* **2006**, *16* (32), 3326−3331.
(20) Liu, Z. P.; Xu, D.; Liang, J.; Shen, J.; Zhang, S.; Qian, Y. *J. Phys. Chem. B* **2005**, *109*, 10699−10704.
(21) Mukherjee, P. K.; Bose, A.; Chakravorty, D. *Appl. Phys. Lett.* **2006**, *89*, 033101.

10.1021/cm0629356 CCC: $37.00
Published on Web 04/17/2007

use of toxic hydrogen sulfide gas, the need for high temperature, the complex processing steps, and the long synthesis time, demand the development of a new synthesis method. In addition, to improve the applicability of these nanorods in nano-opto-electronic devices, we need high-quality, single-crystalline semiconducting nanorods. In this work, we synthesized copper sulfide nanorods by the template-assisted sonoelectrochemistry technique. This method eliminates previously listed undesired limitations and produces single-crystalline semiconducting nanorods.

In addition to benefits provided by ultrasonication, major advantages of electrochemical deposition over other available methods of copper sulfide nanorod production are low operating temperature, environmental friendliness, less time consumption, high reproducibility by control over shape/size, and desired stoichiometry.

Structural properties of nanorods were studied by scanning electron microscopy (SEM, Leo Supra 55 FE-SEM), transmission electron microscopy (TEM, FEI-PHILIPS CM300), X-ray diffraction (XRD, Bruker D8 Advance Diffractometer, Cu Kα radiation, 40 kV, 40 mA), energy-dispersive spectroscopy (EDS), and selected area diffraction (SAD). A UV−Vis spectrophotometer & Agilent 4155C (semiconductor parameter analyzer) with the help of a Signatone probe station were used for optical and electrical characterization of nanorods, respectively.

Experimental Section

Template-assisted electrochemical synthesis of nanorods is explained in detail elsewhere.[2,23] In short, the electrolyte used for electrodeposition was prepared by dissolving $Na_2S_2O_3$ (400 mM) and $CuSO_4$ (60 mM) in DI H_2O. Tartaric acid (75 mM) was used to maintain pH of the solution below 2.5, as required.[24] For the nanorod synthesis, polycarbonate (PC) templates (nominal pore sizes: 200, 100, and 50 nm) were used as working electrodes. A conductive coating of liquid paste of metallic GaIn was applied on the backside of the template. The use of liquid metal is beneficial in two ways; first, it can be easily removed by applying nitric acid,[23] and second, it eliminates the expensive and time-consuming step of metallic layer sputtering. PC templates are advantageous, as they can be easily dissolved in chloroform to liberate nanorods. A platinum spiral rod was used as a counter electrode. Nanorods were prepared by depositing copper sulfide in the template pores at constant potential. The whole electrochemical cell was immersed in an ultrasonicator (Bransonic 2510) containing water. After the nanorods were formed, they were liberated by dissolving the template in chloroform. The solution containing nanorods was cleaned by ultracentrifugation.

Results

Determination of Optimum Deposition Potential. In this research, we standardized the electrodeposition process for copper sulfide nanorods, as there was no report on the same. Determination of optimum potential was of primary importance because of the chronoamperometric electrodeposition process; −0.7 V has been reported in the literature[24] as the appropriate potential for the deposition of copper sulfide films. However, we found out that this value was not suitable for the synthesis of nanorods. As shown in Figure 1a, at the potential to form thin films, there was hardly any formation of nanorods. Cyclic voltammetry experiments were conducted using the PC template as a working electrode to find out the right deposition potential. The optimum potential value standardized for the deposition of nanorods was −1.0 V, and the comparative SEM image of nanorods is shown in Figure 1b.

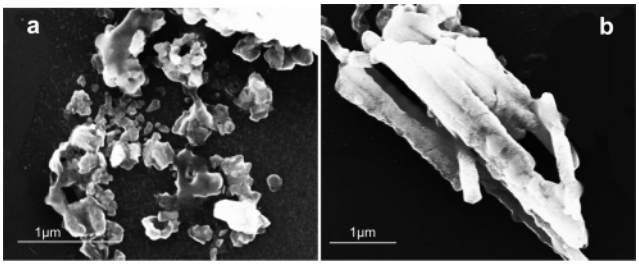

Figure 1. Effect of applied potential on electrodeposition of nanorods. SEM micrographs of the material deposited at (a) −0.7 V (no nanorods) and (b) −1 V (nanorods).

Effect of Ultrasonication on Electrodeposition. An extensive study was conducted to understand the effect of ultrasonication on mass-transfer resistance during electrodeposition. This aspect is of special importance for template-assisted electrochemical deposition. The nanoporous structure of the template, due to its high mass-transfer resistance, hinders the deposition rate and hence uniform and high-quality nanostructures. First, we carefully monitored and calculated the growth rate of nanorods by averaging their lengths at different times for three different methods (Figure 2a). We differentiated between each method of electrodeposition by the external influence used for assisting mass transfer during the deposition process. With the first method, we did not use any other external influence and called it "regular" deposition. The second and third methods were called "stirring" and "ultrasonication" deposition, respectively, indicating the external influence used during electrodeposition. As clearly shown in Figure 2a, higher growth rate of nanorods makes ultrasonication the method of choice. In addition, for better understanding of thermal effects of ultrasonication during electrodeposition, we measured the temperature change for bulk electrolyte for 1 h during sonoelectrochemical deposition and compared it with the corresponding temperature changes for other two methods, regular and stirring (Figure 2b).

It is mentioned in literature[7] that ultrasonication will lower the mass-transfer resistance, but in order to prove it experimentally, we conducted a control experiment. We observed a sudden increase and decrease in the current magnitude directly referring to the corresponding increase and decrease in the resistance, as soon as we switched on/off the ultrasonicator (Figure 2c).

Statistical Analysis of Growth Rate Data and Size Correlation between Template Pore Size and Diameter of the Nanorods. Any data obtained by counting of nanostructures suffer from the limitation of small sample size

(22) Gong, J. Y.; Yu, S. H.; Qian, H. S.; Luo, L. B.; Liu, X. M. *Chem. Mater.* **2006**, *18* (8), 2012−2015.
(23) Bentley, A. K.; Farhoud, M.; Ellis, A. B.; Lisensky, G. C.; Nickel, A. M. L.; Crone, W. C. *J. Chem. Educ.* **2005**, *82* (5), 765−768.
(24) Yukawa, T.; Kuwabara, K.; Koumoto, K. *Thin Solid Films* **1996**, *280* (1−2), 160−162.

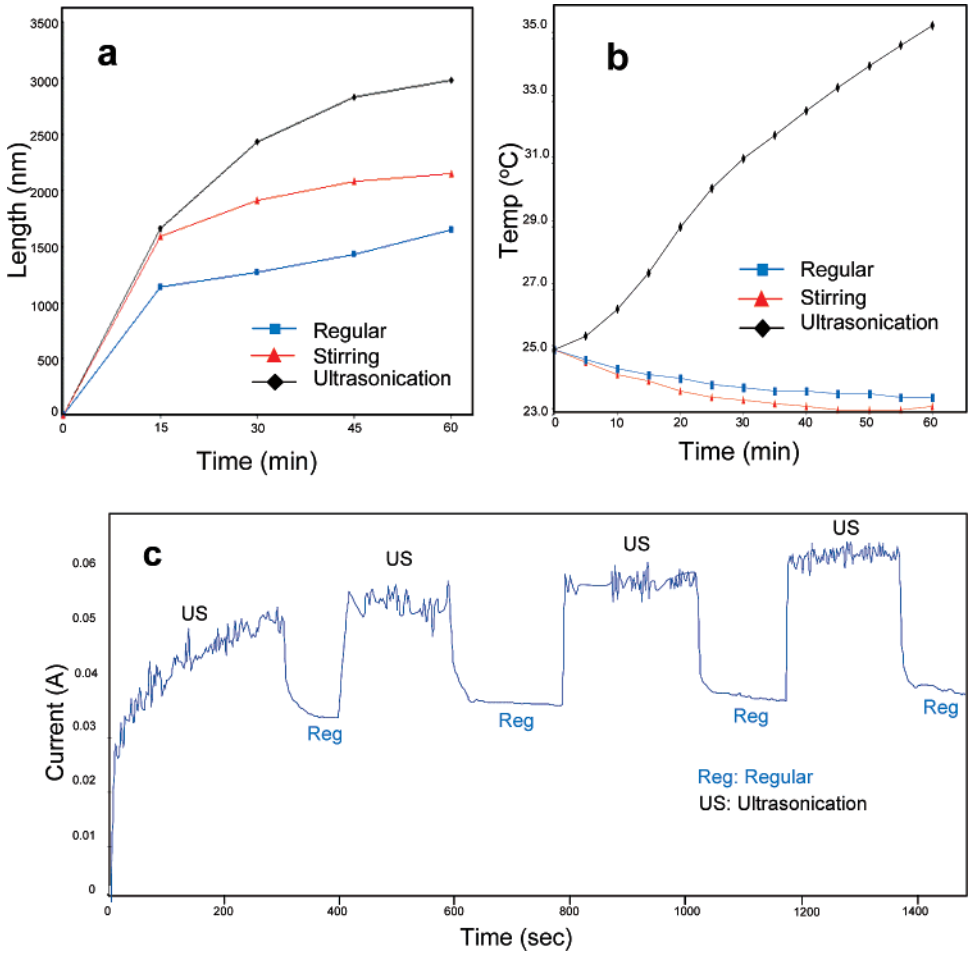

Figure 2. Effect of ultrasonication on electrodeposition. (a) Growth rate of nanorods for ultrasonication, stirring, and regular processes. (b) Temperature rate of bulk electrolyte for same three processes. (c) Effect on resistance provided to electrodeposition by "ultrasonication".

Table 1. Statistical Values for Lengths of Nanorods at Different Times for Different Methods

methods[d]		15 min	30 min	45 min	60 min
R	avg.[a]	1142.6	1272.2	1430.1	1650.8
	S.D.[b]	670	442.2	631.7	657.1
	S.E.[c]	94.7	74.7	83.6	92.9
S	avg.[a]	1588.3	1911.2	2078.2	2146.9
	S.D.[b]	512	444.46	471.06	834.80
	S.E.[c]	72.41	61.63	62.39	109.61
US	avg.[a]	1688.7	2432.7	2832.1	2978.1
	S.D.[b]	750.19	1064.4	1291.2	1125.2
	S.E.[c]	104.0	147.6	171.0	164.1

[a] Average ($\bar{x}$). [b] Standard deviation (s). [c] Standard error: S.E. $= s/\sqrt{n}$, where n = total count. [d] R= regular; S= stirring; US = ultrasonication.

representing a huge population. So, normal statistical parameters like mean, standard deviation, etc., representing the sample also have a high degree of uncertainty. But there are methods available in statistics that help in verifying the data obtained. A two-sample, one-tail z-test[25] was used to compare the difference between the average lengths of nanorods obtained at different times from different methods. Table 1 represents the statistical values for the length data of nanorods. Table 2 provides us the result of the z-test (details in the discussion section), which proves that the data obtained are consistent with the general observation that sonoelectrochemistry results in better deposition. For almost all data points, we obtained $\mu_u > \mu_s > \mu_r$, where μ_u, μ_s, μ_r are the population mean lengths of nanorod samples produced by ultrasonication, stirring, and regular methods, respectively. Data represented in Table 1 and Table 2 was utilized to plot Figure 2a.

As this is a template-based method, size correlation between template surface pore size (D_{mem}) and diameter of nanorods (D_{NR}) is of significant interest. Table 3 represents this size correlation. There was an increase in the ratio (D_{NR}/D_{mem}) with the decrease in D_{mem}. This ratio varies from 1.0 for 200 nm to 1.87 for 50 nm nominal pore size template.

Structural Characterization of Nanorods by Electron Microscopy Techniques. Nanorods prepared sonoelectrochemically were spatially characterized by SEM. Good structural uniformity and high aspect ratio of nanorods are clearly visible in their corresponding SEM micrographs. Figure 3a represents number of nanorods, with nominal diameter of 200 nm. EDS analysis (inset Figure 3b) of a single 200 nm nanorod proves that these rods are made of copper and sulfur (silicon peak is a background signal from Si substrate). To prove the versatility and control of template-assisted synthesis, nanorods with smaller nominal diameters of 100 and 50 nm were also synthesized (images c and d of Figure 3).

TEM in association with SAD, EDS, XRD was employed to understand the stoichiometric composition and crystalline structure of nanorods. SAD patterns (images a and b of

(25) Gupta, S. C.; Kapoor, V. K. *Fundamentals of Mathematical Statistics*; Sultan Chand & Sons: New Delhi, India, 2002.

Table 2. Two-Sample, One-Tail *z*-Test[a] to Compare the Mean Length of the Population (μ)[b] for Nanorods at Different Times for Different Methods

time (min)	R vs S	comparison[c]	S vs US	comparison	conclusion
15	$z = 3.7$ $p = 1 \times 10^{-4}$	$\mu_s > \mu_r$	$z = 0.7$ $p = 0.2$	$\mu_u = \mu_s$	$\mu_u = \mu_s > \mu_r$
30	$z = 6.5$ $p = 0$	$\mu_s > \mu_r$	$z = 3.2$ $p = 1 \times 10^{-4}$	$\mu_u > \mu_s$	$\mu_u > \mu_s > \mu_r$
45	$z = 6.2$ $p = 0$	$\mu_s > \mu_r$	$z = 4.1$ $p = 1 \times 10^{-5}$	$\mu_u > \mu_s$	$\mu_u > \mu_s > \mu_r$
60	$z = 3.4$ $p = 1 \times 10^{-4}$	$\mu_s > \mu_r$	$z = 4.2$ $p = 1 \times 10^{-5}$	$\mu_u > \mu_s$	$\mu_u > \mu_s > \mu_r$

[a] $z = \dfrac{\text{observed difference} - \text{expected difference}}{\text{SE for difference}} = (\bar{X}_1 - \bar{X}_2) - (\mu_1 - \mu_2)\sqrt{\dfrac{\sigma_1^2}{n_1} + \dfrac{\sigma_2^2}{n_2}}$; null hypothesis H_0: $\mu_1 = \mu_2$; alternative hypothesis H_1: $\mu_1 > \mu_2$.
[b] μ = Population mean. [c] μ_r, μ_s, μ_u = Population mean lengths of nanorod samples produced by regular, stirring, and ultrasonication methods, respectively.

Table 3. Size Correlation between Template Surface Pore Size (D_{mem}) and Corresponding Nanorod Sample (D_{NR})

pore size (nm)		membrane	nanorods	D_{NR}/D_{mem}
50	S.D.	20.2	19.2	1.87
	S.E.	2.6	2.2	
	avg.[a]	55.1 ± 5.1	*103.1 ± 4.2*	
100	S.D.	10.96	37.38	1.59
	S.E.	1.60	5.39	
	avg.[a]	84.7 ± 3.1	134.3 ± 10.6	
200	S.D.	51.2	41.0	1.00
	S.E.	6.1	5.9	
	avg.[a]	219 ± 12	219.5 ± 11.49	

[f] Average = mean of the sample ± C.I. (confidence interval); C.I. = z_αS.E; $z_\alpha = 1.96$ for $\alpha = 0.95$, where $z \approx N(0,1)$.

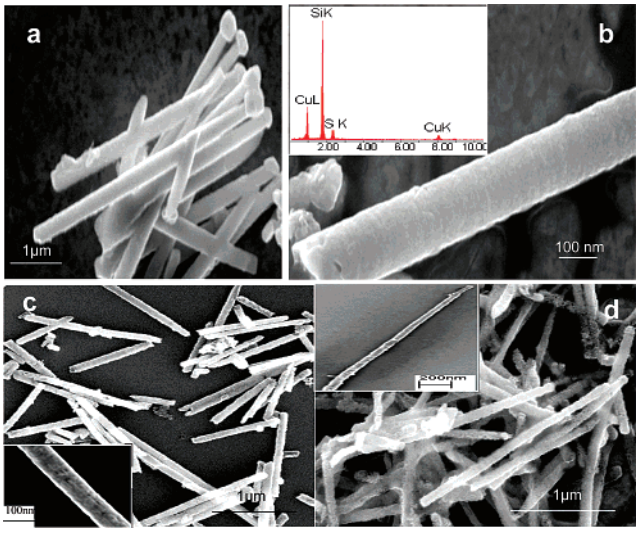

Figure 3. SEM micrographs of nanorods synthesized by sonoelectrochemistry. (a) Nanorods with nominal diameter of 200 nm. (b) EDS analysis of single 200 nm nanorod shows that it contains copper and sulfur only. (c, d) Nanorods with nominal diameters of 100 and 50 nm, respectively. Insets in (c) and (d) confirm the diameter and show the surface structure of an individual nanorod.

Figure 4) obtained after extensive tilting experiments and recording at different orientations from individual nanorod particles along different zone axes reveal that nanorods are single crystals with the covellite structure ($a_0 = 0.379$ nm, $c_0 = 1.636$ nm, S.G. *P*63/*mmc*). The Cu:S ratio in the nanorod sample was determined to vary between 1.0:1.0 and 1.2 :1.0 by EDS analysis (Figure 4f). The XRD pattern for nanorods (Figure 4h) was indexed with CuS structure (JCPDS 06-0464) and a minor amount of $Cu_{1.8}S$ (JCPDS 04-861). High-resolution TEM (HRTEM) images and their corresponding fast Fourier transformation (FFT) patterns were applied to determine the exact crystal structure and symmetry. FFT of Figure 4c confirms the hexagonal symmetry of the crystal. In the same figure, weak satellite spots present along the {110} type of reflection (pointed by arrow) correspond to a periodicity of 0.28 nm and suggest the presence of intergrown domains of cubic $Cu_{1.8}S$ (digenite) ($a_0 = 0.559$ nm, S.G. *Fm*3*m*). Images d and e of Figure 4 demonstrate the high density of structural disorder along the <001> direction, which is expressed as polysynthetic twinning and stacking disorder. Structural characterization by these techniques reveals that nanorods grown sonoelectrochemically have fully crystalline and uniform structure (images h and i (ii) of Figure 4), whereas nanorods produced by regular electrodeposition are polycrystalline and structurally nonuniform (images h and i (i) of Figure 4).

Optical and Electrical Characterization of Nanorods. Optical properties of these nanorods were studied with the help of UV−Vis spectrophotometer at room temperature. Curves a−c of Figure 5a show the absorption spectra of as-prepared nanorods with nominal diameters of 200, 100, and 50 nm, respectively.

To study electrical transport properties and ascertain semiconducting nature, we fabricated a field-effect transistor (FET) device based on an individual copper sulfide nanorod on a SiO_2 wafer by placing the nanorods on pre-patterned gold electrodes. The wafer was used as a universal gate throughout the FET measurements. Figure 5b represents the current−voltage (I_d vs V_d) curve with varying gate voltage (V_g) through a single nanorod ($D \approx 200$ nm, $L \approx 2$ μm) FET. The transport characteristics of the copper sulfide nanorod device were also examined. Figure 5c shows the results of source-drain current versus V_g. Results obtained indicate that these nanorods are p-type semiconductors.

Discussion

As mentioned in results section, we found there was an increase in the applied potential (−0.7 to −1 V) for nanorods in comparison to that reported for films.[24] We attribute this increase to the increased resistance provided to deposition in pores of PC template. Qualitatively, the applied potential (E_{appl}) differs from the equilibrium potential (E_{eq}) by overpotential, η[26]

(26) Bard, A. J.; Faulkner, L. R. *Electrochemical Methods: Fundamentals and Applications;* John Wiley & Sons: New York, 1980.

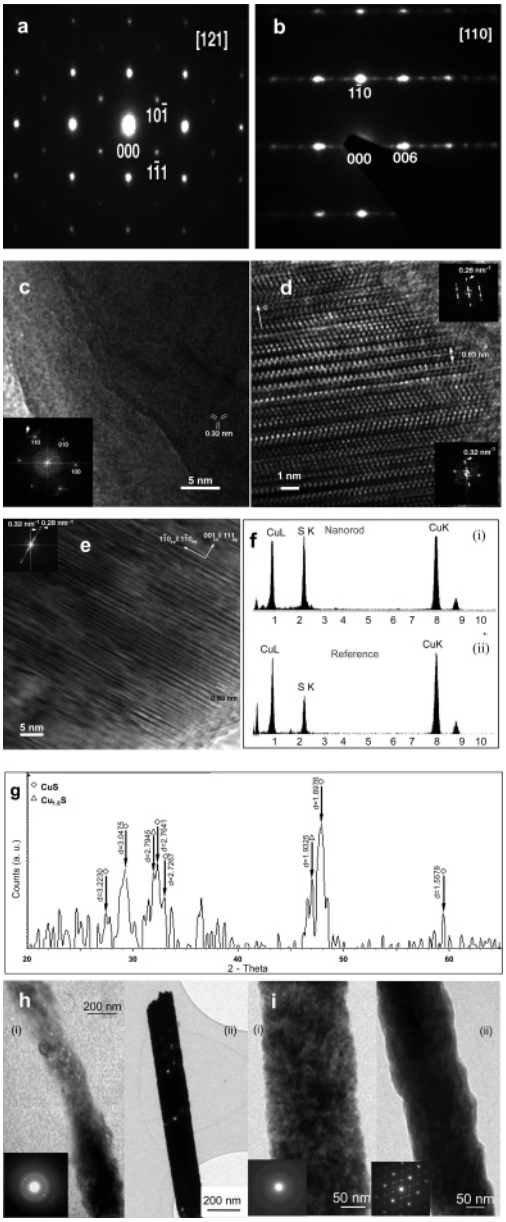

Figure 4. Structural characterization of CuS nanorods produced sonoelectrochemically. Typical SAD patterns (a, b) taken from a single nanorod particle clearly show that nanorods are single crystals with the covellite structure (a_0 = 0.379 nm, c_0 = 1.636 nm, S.G. *P*63/*mmc*). The first (a) pattern was taken along the [121] zone axis. The second one (b) corresponding to the [110] zone axis shows pronounced streaking of the reflections along the <001> direction (c) HRTEM image of single nanorod taken along the [001] zone axis. FFT pattern (inset) confirms the hexagonal symmetry of the crystal. Weak satellite spots present along the {110} type of reflection (pointed by arrow, periodicity 0.28 nm) corresponds to intergrown domains of cubic $Cu_{1.8}S$ (a_0 = 0.559 nm, S. G *Fm*3*m*). (d) HRTEM image of a nanorod (zone axis [010]). FFT patterns, top (corresponds to upper part of the image) and bottom (corresponds to the lower left part) insets, show covellite CuS and digenite Cu_2S structures, respectively. The image also demonstrates the high density of structural disorder along the <001> direction. (e) HRTEM image of a nanorod (zone axis[110]). FFT pattern (inset) reveals the presence of digenite lamellae intergrown with covellite parallel to {001}. (f) EDS spectra of CuS nanorods (i) and standard synthetic crystal of tetragonal Cu_2S (ii). Using the Cu_2S as a standard the Cu:S ratio in the nanorod sample was determined to vary between 1.0:1.0 and 1.2:1.0. (g) XRD pattern for nanorod indexed with CuS structure (JCPDS 06-0464) with a minor amount of $Cu_{1.8}S$ (JCPDS 04-861). (h) TEM micrographs (i) showing the nonuniform and polycrystalline (SAD pattern in inset) structure of a typical nanorod produced by regular electrochemical deposition and (ii) representing a typical uniform nanorod produced sonoelectrochemically. (I) TEM micrographs of nanorods after 15 min of (i) regular and (ii) sonoelectrochemical deposition. Inset (i) and (ii) show corresponding SAD patterns.

$$\eta = E_{\text{appl}} - E_{\text{eq}} \tag{1}$$

This overpotential is the sum of different overpotential terms associated with different reaction steps.[25] Mass transfer being one of the reaction steps contributes to overpotential (η_{mt}). The nanoporous structure of the PC template increases the mass-transfer resistance, which in turn increases the corresponding overpotential. Hence, mass-transfer resistance increases the applied voltage.

A detailed analysis of the effects of ultrasonication on the template-assisted electrodeposition is provided in this section. We strongly believe that this discussion will be useful for applying sonoelectrochemical process not only for synthesis of copper sulfide nanorods, but in general for template-assisted electrochemical synthesis of 1D nanostructures. A faster deposition rate of ultrasonication process (Figure 2a) results from the cavitation phenomena as well as the effects of propagation of acoustic waves in the liquids. The maximum radius of collapsing bubbles under constant pressure can be calculated from eq 2[27]

$$R_{\text{max}} = (3 \times 10^3/f)(P_a - 1)(P_a)^{-1/2}[1 + 2(P_a - 1)/3]^{1/3} \tag{2}$$

where f (kHz) is acoustic field frequency and P_a (atm) is the acoustic pressure, which in turn can be calculated from acoustic intensity I_a (eq 3)[27]

$$P_a = (2\rho c_L I_a)^{1/2} \tag{3}$$

where ρ and c_L stand for medium density and speed of sound in that medium, respectively.

For our ultrasonicator (f = 40 kHz and $I_a \approx$ 2.5 W/cm^2), the calculated radius of the collapsing bubble was around 90 μm. This bubble radius is much greater than the pore size of the template. Obviously, this particular size of bubble can never collapse in the interior section of pores in order to build up the local turbulence. But the collapse of these bubbles inside the liquid generates intensive shock waves, and the transient high pressure from the shock waves probably prevents plugging of the nanopores, which enhances the mass-transfer rate.[28] In addition, ultrasonic waves generate very high acoustic pressures P_a (eq 3). On the basis of the intensity of ultrasonicator used, P_a as high as 2.5 atm can be generated inside the liquid. Vradman et al.[28] state that this high pressure produces an acoustic capillary effect, i.e., the rate of liquid streaming is considerably accelerated inside the thin capillaries under the effect of ultrasound, even in the absence of local cavitation. In fact, this absence of cavitation inside the pores is most probably helpful in preventing the direct damage to the structure of deposited material. Cavitation, being a high-energy process, may result in physical damage to the nanorods if it is happening inside the pores.

(27) Colussi, A. J.; Weavers, L. K.; Hoffmann, M. R. *J. Phys. Chem. A* **1998**, *102* (35), 6927−6934.
(28) (a) Vradman, L.; Landau, M. V.; Herskowitz, M.; Ezersky, V.; Talianker, M.; Nikitenko, S.; Koltypin, Y.; Gedanken, A. *Nanotechnol. Mesostruct. Mater.* **2003**, *146*, 721−724. (b) Suslick, K. S.; Hammerton, D. A.; Cline, R. E. *J. Am. Chem. Soc.* **1986**, *108* (18), 5641−5642.

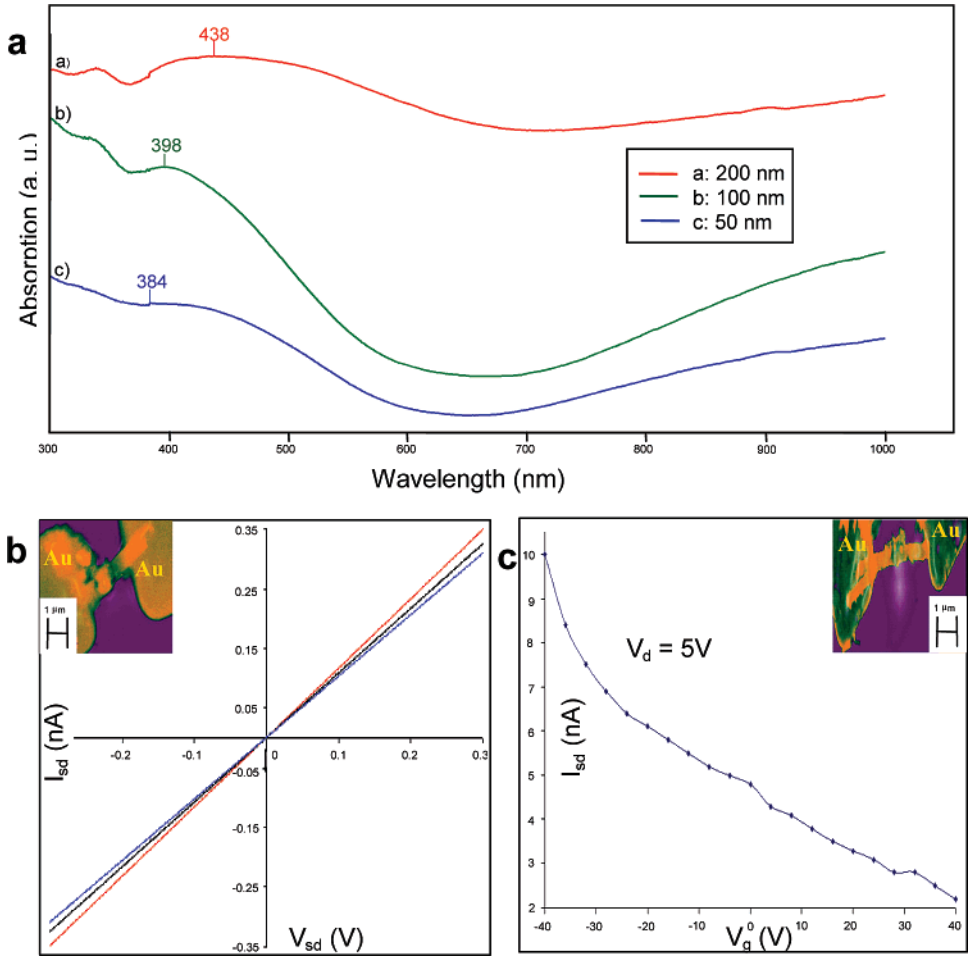

Figure 5. Optical and electrical characterizations of nanorods. (a) Absorption spectra of (a) 200, (b) 100, and (c) 50 nm nanorods. (b) Gate-dependent $I_{sd}-V_{sd}$ curves from a single CuS nanorod field effect transistor (FET). −40 V (red line), 0 V (black line), 40 V (blue line). (c) I_{sd} versus V_g curve showing that copper sulfide nanorod device operates as p-channel MOSFET. (Inset for b, c: SEM images of corresponding single nanorod FET. The figures have been artistically enhanced for better visibility. Scale bar 1 μm.)

In addition to the physical effects (lowering the mass-transfer barrier), the thermal effects (increasing the reaction rate) of ultrasonication have also played a significant role in the improved deposition rate (Figure 2a). The enormous local temperature, pressure, and the extraordinary heating and cooling rates[28] generated by cavitational collapse result in high-energy chemistry. Like photochemistry, very large amounts of energy are introduced in a short period of time, in this case, thermal not electronic. Therefore, it is suggested that one might be able to produce on a microscopic scale the same macroscopic conditions of high temperature and pressure.[6] This localized thermal effect enhances the chemical reaction rate and gives rise to the term "sonochemistry". In our case, these effects become more pronounced in the later part of the deposition (Figure 2a). In fact, initially, there is no major difference between stirring (another physical phenomenon) and ultrasonication. We conclude that the initial outcome of thermal effects on deposition rate was not as pronounced as a major part of ultrasound energy was used in degassing solution and cleaning electrodes. But once that action is complete, thermal effects in addition to physical effects of ultrasound started contributing toward enhancing the deposition rate. To directly observe the effect of thermal energy dissipation during ultrasonication, we measured the change in temperature of bulk electrolyte for all three processes, ultrasonication, stirring, and regular (Figure 2b). We observed a temperature increase of around 11 °C for sonoelectrochemical deposition, which was significantly higher than the corresponding change (∼1−2 °C) for the other two methods. This observation also supports the role of thermal effects during sonoelectrochemical deposition.

The effect of ultrasonication on mass-transfer resistance was directly observable during electrodeposition. It is clearly shown in Figure 2c that the magnitude of deposition current increases with the initiation of ultrasonication. Because the voltage applied is constant, this increase comes from the decrease in the resistance. As all other factors are same, this decrease corresponds to the reduction in mass-transfer resistance inside the pores during the sonoelectrochemical deposition process.

Generally, nanomaterials are produced in very large quantities; for example, electrodeposition produces millions of nanorods simultaneously. But for the mathematical analysis, one can sample up to few hundred nanostructures at most. Therefore, normal sample parameters like mean and standard variation are not very representative of the whole population. In this work, we have compared the growth rate of different methods (Figure 2a). For greater certainty, the sample parameters obtained alone cannot suffice. Therefore, a two-sample, one-tail *z*-test[25] was employed to compare the

difference between the average lengths of nanorods obtained at different times from different methods. The results are tabulated in Table 2. The *z*-test is explained in detail elsewhere.[25] In short, we assume a Null hypothesis to be true (H_0: $\mu_1 = \mu_2$), which corresponds to equality between the means of population 1 and 2. In our case, it means that the average lengths of different methods are comparable and we cannot say with certainty that one process results in longer nanorods. To prove otherwise, an alternative hypothesis is chosen that is true when Null hypothesis is rejected. the alternative hypothesis chosen here was (H_1: $\mu_1 > \mu_2$), implying that the mean length of nanorods produced by process 1 is greater than the other. We use a one-tail test to leave out the possibility of $\mu_1 < \mu_2$. The formula for calculating *z* is given in Table 2. Once we obtain *z*, the probability value (p-value = P[Obs $z > z$]) was calculated from it by *z*-table distribution.[25] The test utilizes the p-value to reject ($p \leq 0.05$) or accept ($p > 0.05$) the null hypothesis.[25] Statistical analysis proved that for all but one point ($\mu_u > \mu_s > \mu_r$), sonoelectrochemical deposition results in longer nanorods and hence better deposition rate. The only point where $\mu_u = \mu_s$ was after the first 15 min of deposition. This is also consistent with the experimental observation, and the underlying reason has already been explained. But even at this point, ultrasonication/stirring results in longer nanorods than regular deposition.

In this study, size correlation was established between the template surface pore size and diameter of nanorods produced (Table 3). As previously reported,[29] we also found that as the nominal pore size of the template decreases, the size correlation ratio D_{NR}/D_{mem} increases. This does not imply that nanorods are not representative of pore shape and size. In fact, pore shape changes with nominal pore size of the template.[29] Due to the proximity effect[30] during the production of these ion track-etched templates, pores are widened below the template surface; this effect is more pronounced for smaller pore sizes.[29]

Structural analysis of nanorods was of special importance, as one of the major aims of this work is to demonstrate the superior structural quality of nanorods produced sonoelectrochemically. Because copper sulfide crystallizes in a large number of structurally very closely related phases[31] with very similar lattice parameters, the exact structural and compositional analysis of the nanorod specimens was a very complex task. This was further complicated by the presence of a high density of planar defects in the crystals. Reliable identification of the structure of the nanorods was obtained only after performing extensive tilting experiments and recording several SAD patterns from individual nanorod particles along different zone axes. After this, stereographic projections were utilized to compare the experimental angles of tilt with the theoretical angles between zone axes for a range of copper sulfide structures. This procedure allowed us to determine with absolute reliability the 3D structure of nanorod specimen, which belongs to the hexagonal covellite structure ($a_0 = 0.379$ nm, $c_0 = 1.636$ nm, S.G. $P6_3/mmc$).[32] The SAD patterns (images a and b of Figure 4) obtained from individual nanorods consist of discrete diffraction spots related to each other by translational symmetry, which confirms the single-crystal nature of the nanorods. There is significant planar disorder in most of the crystals, which is expressed as heavy streaking of the reflections along <001> in zone axis orientations normal to the *c*-axis (Figure 4b). The nature of the disorder was revealed by HRTEM imaging (Figure 4c−e). In orientations for which the electron beam is not normal to the *c*-axis (Figure 4c), the covellite crystal lattice exhibits perfect order with minor distortions due to the presence of cubic digenite ($Cu_{1.8}S$) domains ($a_0 = 0.559$ nm, S.G $Fm3m$).[33] In contrast, for orientations normal to the *c*-axis, a high density of planar defects is observed, which forms a domain structure with one-dimensional disorder along the *c*-axis expressed as stacking faults, polysynthetic twinning on {001}, and intergrown domains of digenite (images d and e of Figure 4). The size of the individual domains separated by stacking faults and twin planes is just a few nanometers along the *c*-axis and they extend almost uninterrupted along the entire length of the nanorods, which is normal to the *c*-axis.

The composition of the nanorods was determined by EDS analyses (Figure 4f), using commercially available synthetic crystal of Cu_2S (Sigma Aldrich) as a standard reference. We found that the Cu:S ratio in the nanorods varies between 1.0:1.0 and 1.2:1.0, which is consistent with the data from electron diffraction and HRTEM experiments.

These samples were further analyzed by XRD. The XRD pattern (Figure 4g) was indexed with the CuS structure (JCPDS 06-0464) with small amount of digenite, $Cu_{1.8}S$ (JCPDS 04-861). It should be pointed out that because of the presence of significant planar defects in the crystals, the match with XRD patterns from pure, well-crystallized, defect-free phases can be misleading and is not expected to be accurate. The small domain size along the *c*-axis, as established by HRTEM, will prevent reflections of {00l} type from developing and may lead to incorrect conclusions about the actual structure of the nanorods. The theoretically strongest reflection for covellite (103) at 2.8 Å may be missing or reduced in intensity because of the planar disorder along the *c*-axis. In addition, reflections of type {hk0} could become unusually strong, because they will not be affected by the planar disorder along *c*. Thus, the (110) reflection in covellite at 1.89 Å could become the strongest reflection, which is exactly what was observed in our experimental XRD patterns, indirectly confirming the findings by electron microscopy. We also emphasize that obtaining a pure phase of XRD is not possible for various reasons, such as pore size difference for the same template, variable mass-transfer resistance, and structurally very closely related phases of copper sulfide (Cu_xS, $1 < x < 2$).

Because of the bulk nature of the electrodeposition process, producing perfectly crystalline nanorods without any kind

(29) Schonenberger, C.; vanderZande, B. M. I.; Fokkink, L. G. J.; Henny, M.; Schmid, C.; Kruger, M.; Bachtold, A.; Huber, R.; Birk, H.; Staufer, U. *J. Phys. Chem. B* **1997**, *101* (28), 5497−5505.
(30) Hatzakis, M. *IBM J. Res. Dev.* **1988**, *32* (4), 441−453.
(31) Börnstein, L. *Non-tetrahedrally Bonded Elements and Binary Compounds I*;. Springer: Berlin, Germany, 1998.
(32) Berry, L. G. *Am. Mineral.* **1954**, *39*, 504−509.
(33) Will, G.; Hinze, E.; Abdelrahman, A. R. M. *Eur. J. Mineral.* **2002**, *14*, 591−598.

of structural defects is nearly impossible. But still, ultrasonication is primarily responsible for the nearly perfect crystalline structure of the nanorods along directions normal to the *c*-axis. On the other hand, nanorods prepared by the regular method were found to be genuinely polycrystalline in nature (insets of panels h and i (i) of Figure 4). The main reason for this is the physical assistance provided by ultrasonication during electrodeposition. The unplugging of pores during sonoelectrochemical deposition as discussed above results in uniform deposition in comparison to regular electrochemical deposition. Superior structural uniformity is clearly shown in the TEM micrograph (images h and i (ii) of Figure 4) of a typical nanorod produced sonoelectrochemically.

Sonoelectrochemical deposition also satisfies the conditions favorable for producing a single-crystalline structure by electrodeposition. During electrochemical deposition, new grains will grow if the size of an initial cluster exceeds the critical dimension N_c.[34] The larger the N_c, the more favorable it is for a single crystal to grow from a previously nucleated seed grain. The critical dimension N_c for a 2D-like nucleus can be expressed as

$$N_c = bs\epsilon^2/(Ze\eta)^2 \quad (4)$$

where s, ϵ, Z, η, and b are the area occupied by one atom on the surface of the nucleus, the edge energy, the effective electron number, the overpotential, and a constant, respectively. The assumption regarding 2D single-crystalline structure is also satisfied by HRTEM studies, where we found that the nanorods have single-crystalline structure in 2D with planar disorder along *c*. During electrodeposition, the only parameter that we can change is the overpotential η. If η is low, then single-crystal growth is favored because N_c is large.[34] The reduction in η is clearly shown during sonoelectrochemical deposition (Figure 2c). We have clearly proved that the reduction in deposition resistance for ultrasonication is directly attributed to a decrease in mass-transfer resistance. As η includes a mass-transfer resistance term as well,[26] its decrease lowers the overpotential as well. Hence low η for US in comparison to regular electrodeposition is mainly responsible for formation of single-crystal nanorods.

The increase in temperature may help in the formation of single crystal,[34] as it promotes the surface diffusions of atoms and favors the growth of preexisting nuclei of nanorods; however, this alone is not sufficient. In fact, there is a conflicting report[35] suggesting that thermal energy agitates the growth and distorts the competition between adjacent grains, resulting in polycrystallinity. We believe that the lowering of η is more important for our system, because we have compared the products not only after 1 h of production (Figure 4h) but also after 15 min (Figure 4i). As mentioned above, we found that nanorods produced sonoelectrochemically were single crystal, even after the first 15 min of deposition. At this time, there is an increase of only 1.5 °C in temperature for the ultrasonication method.

Copper sulfide is primarily used as a component for photovoltaics and therefore the optical properties of its nanorods are of significant importance. Previous studies[36] have shown that CuS has a characteristic absorption band in near-IR region. Our observance is also in agreement with this. For all (a) 200, (b) 100, and (c) 50 nm nanorod samples, we observed a wide absorption band beyond 800 nm. It is also reported[16] that peaks observed around 400 nm could be attributed to the nanorod morphology of the particles. In fact, a decrease in the size of the particles leads to an increase in blue shift due to size quantization effect.[36] In our case, we see peaks corresponding to nanorod structures around 438, 398, and 384 nm for curves a−c, respectively. Though the radius of nanorods is greater than the typical Bohr radius of semiconductors (∼2−60 nm),[37] size quantization can be plausibly explained by following two arguments. First, it has been reported[38] that when the average radius of the nanoparticles (R) is much greater than the exciton Bohr radius (a_B) of the bulk semiconductor ($R \gg a_B$), the coulomb energy is dominant and motion of the exciton experiences size quantization. Therefore, the character of exciton as a quasiparticle is preserved, only its translational degrees of freedom are modified, resulting in a small increase in the exciton energy. The features in the optical spectra move slightly to the blue, as seen in the absorption spectra of CuS nanorods. This also explains the less-pronounced hump in the absorbance spectrum rather than a sharp peak. Second, sonoelectrochemistry is a bulk process that includes nanorods as well as small crystals in the final product. Most likely, not all the nanocrystals convert into nanorods and some phases of the rods remain within the Bohr radius (or at least comparable). We expect that these nanocrystals show some size quantization effect and contribute to the slight blue shift observed in the absorbance spectrum of our CuS nanorods. Therefore, the trend of increased blue shift (from 438 nm for 200 nm diameter rods to 384 nm for 50 nm diameter rods) corresponding to smaller diameter of the nanorods is an indication of size quantization effect. But the proportional increase in blue shift from 100 to 50 nm is not so pronounced as from 200 to 100 nm because the ratio D_{NR}/D_{mem} is relatively higher for 50 nm templates compared to other two (200 and 100 nm).

Semiconductor nanorods are of great importance for application in future nano-opto-electronic devices.[39,40] Synthesis of semiconducting nanorods has been widely researched.[40] But it is imperative to understand the electrical transport properties of individual nanorods, for their application in nanolevel electronic circuits. This work is where the

(34) Tian, M. L.; Wang, J. U.; Kurtz, J.; Mallouk, T. E.; Chan, M. H. W. *Nano Lett.* **2003**, *3*, 919−923.
(35) Pan, H.; Liu, B.; Yi, J.; Poh, C.; Lim, S.; Ding, J.; Feng, Y.; Huan, C. H. A.; Lin, J. *J. Phys. Chem. B* **2005**, *109*, 3094−3098.
(36) (a) Haram, S. K.; Mahadeshwar, A. R.; Dixit, S. G. *J. Phys. Chem.* **1996**, *100* (14), 5868−5873. (b) Dixit, S. G.; Mahadeshwar, A. R.; Haram, S. K. *Colloids Surf., A* **1998**, *133* (1−2), 69−75. (c) Xu, H. L.; Wang, W. Z.; Zhu, W. *Mater. Lett.* **2006**, *60* (17−18), 2203−2206.
(37) Buhro, W. E.; Colvin, V. L. *Nat. Mater.* **2003**, *2* (3), 138−139.
(38) Yoffe, A. D. *Adv. Phys.* **2002**, *51* (2), 799−890.
(39) (a) Wang, W. U.; Chen, C.; Lin, K. H.; Fang, Y.; Lieber, C. M. *Proc. Natl. Acad. Sci., U.S.A.* **2005**, *102* (9), 3208−3212. (b) Karnik, R.; Fan, R.; Yue, M.; Li, D. Y.; Yang, P. D.; Majumdar, A. *Nano Lett.* **2005**, *5* (5), 943−948.
(40) (a) Sirbuly, D. J.; Law, M.; Yan, H. Q.; Yang, P. D. *J. Phys. Chem. B* **2005**, *109* (32), 15190−15213. (b) Mao, C. B.; Solis, D. J.; Reiss, B. D.; Kottmann, S. T.; Sweeney, R. Y.; Hayhurst, A.; Georgiou, G.; Iverson, B.; Belcher, A. M. *Science* **2004**, *303* (5655), 213−217.

electric transport studies were first conducted on individual copper sulfide nanorods. Figure 5b represents the current−voltage (I_d vs V_d) with varying gate voltage (V_g) through a single nanorod ($D \approx 200$ nm, $L \approx 2$ μm) FET, fabricated by placing individual nanorods across prepatterned gold microelectrodes. The transport characteristics of the copper sulfide nanorod device were also examined. Figure 5c shows the results of source-drain current versus V_g. As shown in Figure 5b, conductance slightly increases with increasing negative gate voltage, which indicates that copper sulfide nanorods are weakly p-type semiconductors. It should be noted that the effect of the gate voltage is significantly reduced by the high oxide thickness of the wafer and unavoidable large contact resistance between the nanorod and electrode surfaces. This observance of hole-dominated conductance is in accordance with those reported in literature for copper sulfide[41,42] and comes from the fact that copper vacancies in the material act as acceptors making copper sulfide a p-type semiconductor. Figure 5c represents the transport characteristic of as prepared copper sulfide nanorod device. It can be deduced from Figure 5c that the device operates as p-channel metal-oxide semiconductor FET (saturation of the conductance could not be reached because of high contact resistances and poor gating of the transistor because of the high oxide thickness).

Conclusion

In conclusion, we synthesized copper sulfide nanorods by the sonoelectrochemical deposition method. This method results in faster production of high-quality, one-dimensional nanostructures. Nanorods produced were single crystals of covellite (CuS) having hexagonal symmetry. Absorbance studies of nanorods are in accordance with literature showing size quantization effects. Electrical characterization of single nanorods confirms their p-type semiconducting nature. Because of their good structural and electrical properties, these nanorods are a suitable candidate for application in future nano-opto-electronic devices. The template-assisted sonoelectrochemical deposition method demonstrated is not limited to any particular kind of nanorods but can be utilized for synthesis of different materials with varying geometry. Though there is a report on producing single-crystal nanowires by electrodeposition,[43] it requires a high salt concentration and fine-tuning of the electrical and structural properties of the template. But sonoelectrochemistry being a thermophysical phenomenon can be used regardless of the chemistry, composition of the electrolyte or charge on the electrode to produce high quality single crystalline one-dimensional structures. In fact, we believe this detailed study on the potential benefits of ultrasonication during electrodeposition would immensely help the scientific community working in this field.

Acknowledgment. We thank to the SCPPA, the UCEI, and the FCRP-DARPA-FENA center for financial support. Authors acknowledge the help of F. Yilmaz in the electrical characterization of nanorods. The authors also thank Dr. S. Walker and D. Dey for participating in our discussions.

CM0629356

(41) Okamoto, K.; Kawai, S. *Jpn. J. Appl. Phys.* **1973**, *12* (8), 1130.
(42) Dittmer, W. U.; Simmel, F. C. *Appl. Phys. Lett.* **2004**, *85* (4), 633−635.
(43) Zhang, X.; Yao, B.; Zhao, L.; Liang, C.; Zhang, L.; Mao, Y. *J. Electrochem. Soc.* **2001**, *148* (7), G398−G400.